Radius of ^{8}B halo from the asymptotic normalization coefficient

F. Carstoiu,[1,2] L. Trache,[1] C. A. Gagliardi,[1] R. E. Tribble,[1] and A. M. Mukhamedzhanov[1]
[1]*Cyclotron Institute, Texas A&M University, College Station, Texas 77843*
[2]*Institute of Atomic Physics, P. O. Box MG-6, Bucharest, Romania*
(Received 22 January 2001; published 19 April 2001)

The experimental asymptotic normalization coefficient determined from peripheral transfer reactions is used to obtain the root-mean-square radius of the wave function for the loosely bound proton in ^{8}B. It is shown that the asymptotic region contributes most and that matching of the interior wave function with the asymptotic part yields a nearly model-independent radius. We obtain $\langle r^2\rangle^{1/2}=4.20\pm0.22$ fm for the root-mean-square (rms) radius of the last proton, much larger than the rms radius of the ^{7}Be core. This large value and the fact that the asymptotic part of the proton wave function contributes 85% to the rms radius are good sign that ^{8}B is a halo nucleus.

DOI: 10.1103/PhysRevC.63.054310 PACS number(s): 21.10.Gv, 21.10.Dr, 24.10.−i, 27.20.+n

The proton drip line nucleus ^{8}B has a very small one-proton separation energy ($S_p=137$ keV) and the valence-proton wave function is expected to penetrate substantially beyond the range of the nuclear force. The penetration is hindered by the combined effect of Coulomb and centrifugal barriers. Many experiments have been devoted to studies of ^{8}B in order to establish its halo nature. These include the determination of the interaction cross section [1,2], quasi-elastic scattering [3], reaction cross section [4,5], electric quadrupole moment [6], nuclear breakup [5,7], and Coulomb dissociation [8–10]. Interaction and reaction cross section measurements are particularly important since these observables can be directly related to the nuclear size. The parallel momentum distribution for corelike fragments in breakup reactions is also easily related to size since it is a direct mapping of the Fourier transform of the halo wave function, slightly modified by final-state interactions [11–14].

The asymptotic normalization coefficient (ANC) for $^8\mathrm{B}\rightarrow{}^7\mathrm{Be}+p$, specifying the amplitude of the tail of the ^{8}B wave function projected on the two-body channel $^7\mathrm{Be}+p$, has recently been determined using the peripheral proton transfer reactions $^{10}\mathrm{B}(^7\mathrm{Be},^8\mathrm{B})^9\mathrm{Be}$ [15] and $^{14}\mathrm{N}(^7\mathrm{Be},^8\mathrm{B})^{13}\mathrm{C}$ [16]. An analysis [17] of uncertainties in these two reactions yielded a weighted average ANC $C^2_{p_{3/2}}=0.388\pm0.039$ fm^{-1}. In the following, we examine the possibility of using this experimental ANC to obtain information on the root-mean-square (rms) radius of the wave function. We begin by recalling the definition of the ANC, and then examine its relationship to the nuclear size.

The overlap integral of the bound-state wave functions for particles A, p, and B, where $B\equiv(Ap)$ is a bound state of nucleus A and proton p, is given by [18,19]

$$I^B_{Ap}(\vec{r})=\langle\mathcal{A}[\varphi_A(\xi_A)\varphi_p(\xi_p)]\,|\,\varphi_B(\xi_A,\xi_p,\vec{r})\rangle$$
$$=\sum_{l_B,m_{l_B}j_Bm_{j_B}}\langle J_AM_Aj_Bm_{j_B}|J_BM_B\rangle$$
$$\times\langle J_pM_pl_Bm_{l_B}|j_bm_{j_B}\rangle i^{l_B}Y_{l_Bm_{l_B}}(\hat{r})I^B_{Apl_Bj_B}(r). \quad (1)$$

$\mathcal{A}$ is the antisymmetrization operator, φ is a bound-state wave function, ξ is a set of internal coordinates including spin-isospin variables, and $\vec{r}$ is the vector connecting the center of mass of nucleus A with p. In the second line, the antisymmetrization factors have been absorbed in the radial overlap integrals $I(r)$. The multipole expansion is carried out over l_B,j_B values allowed by angular momentum and parity conservation for the virtual process $B\rightarrow A+p$. The overlap integral is not an eigenfunction of the total Hamiltonian, and hence, it is not normalized to unity. The square of the norm of the overlap integral

$$S_{Ap}=\int d\vec{r}[I^B_{Ap}(\vec{r})]^2 \quad (2)$$

is by definition the spectroscopic factor. Its value depends on the specific model for the bound states and on the magnitude of the antisymmetrization effects that connect different non-orthogonal channels. Inside the core of the nucleus the overlap integral involves many-body functions, and it may be difficult to calculate. At asymptotic distances where nuclear forces are vanishingly small, $r>R_N$, the overlap integral behaves as

$$I^B_{Apl_Bj_B}(r)\rightarrow C^B_{Apl_Bj_B}\frac{W_{\eta_B,l_B+1/2}(2k_Br)}{r}. \quad (3)$$

Here $C^B_{Apl_Bj_B}$ is the asymptotic normalization coefficient defining the amplitude of the tail of the overlap integral, W is the Whittaker function obtained by solving the Schrödinger equation for two charged particles at negative energy $\epsilon_B=-S_p$, $k_B=\sqrt{-2\mu_{Ap}\epsilon_B/\hbar^2}$ is the wave number, μ_{Ap} is the reduced mass of particles A and p, and η_B is the Sommerfield parameter for the bound state (Ap).

In the case of the ^{8}B ground state, the last proton is mostly in the $1p_{3/2}$ and $1p_{1/2}$ orbitals. Here the halo radius can be correlated to the ANC in a very simple way. Indeed, after integrating over the angular part, the rms radius of the wave function of the last proton becomes (e.g., [20,21])

$$r_h^2 = \int_0^\infty r^4 dr I_g^2(r) + \int_0^\infty r^4 dr I_e^2(r) + \cdots = r_g^2 + r_e^2 + \cdots, \tag{4}$$

where $I_g(r)$ and $I_e(r)$ are the overlap integrals arising from the parts of the ^{8}B ground-state wave function where the proton orbits the ground and excited states of the ^{7}Be core, respectively. The first term dominates. For it we can further write, separating the contributions of the interior and the asymptotic region,

$$r_g^2 = \int_0^{R_N} r^4 dr I_g^2(r) + C_{eff}^2 \int_{R_N}^\infty r^2 dr W^2(2k_B r). \tag{5}$$

Here we take an effective ANC $C_{eff}^2 = C_{p_{3/2}}^2 + C_{p_{1/2}}^2$ because the radial behavior of the $p_{3/2}$ and $p_{1/2}$ orbitals is the same at large radii. We use the theoretical estimate $C_{p_{1/2}}^2 / C_{p_{3/2}}^2 = 0.157$, as in [15,16] and the experimental value for $C_{p_{3/2}}^2$ to obtain $C_{eff} = 0.670 \pm 0.034$ fm$^{-1/2}$. From this we can evaluate the rms radius of the wave function of the last proton in ^{8}B.

First we employ the same procedure that we used in the determination of the ANC from the (^{7}Be,^{8}B) transfer reactions and calculate single-particle wave functions in typical Woods-Saxon potentials. We vary the reduced radii r_0 and the diffuseness a of the potential on a grid of $4 \times 3 = 12$ points for $r_0 = 1.0$–1.3 fm and $a = 0.5$–0.7 fm with 0.1 fm steps and add a (somewhat arbitrary) point at $r_0 = 1.13$ fm and $a = 0.55$ fm. The depth of the potential is adjusted to reproduce the binding energy of ^{8}B at $\epsilon_B = -137$ keV. This is very important in order to obtain the correct asymptotic behavior for the wave functions. With these single-particle wave functions, the rms radius predicted for the $1p_j$ orbital varies anywhere between 3.84 and 4.66 fm. However, these single-particle wave functions, which are all normalized to unity, fail to reproduce the experimental ANC. In contrast, requiring the overlap integrals in Eq. (5) to have the asymptotic behavior given by the ANC extracted from experiment produces an average value of $\langle r_g^2 \rangle_{av}^{1/2} = 3.98$ fm over the 13 points, with a standard deviation of only 0.08 fm. With this procedure all the overlap integrals are identical at large distances, but may differ in the interior of the nucleus. However, the predicted rms radii are nearly identical, varying much less than the uncertainty of $\delta \langle r^2 \rangle^{1/2} = 0.20$ fm induced by the 5% experimental error in the determination of the ANC itself. This is essentially due to the fact that the asymptotic region of the wave function gives the major contribution to the rms radius. The region at radii larger than $R = 4.0$ fm contributes 23–33 % to the norm of the wave function, but it contributes an average of 86% to the rms radius. Thus, the error we make by replacing in the first term of Eq. (5), the (unknown) overlap integral in the interior, with the wave functions calculated above is small, but it is very important to use the correct function at large distances. Moreover, the result that the region outside the core radius contributes most justifies the use of a single-particle overlap integral. Microscopic calculations [21–23] also conclude that the many-body overlap integrals are close to two-body potential-model wave functions calculated in standard Woods-Saxon geometries and, therefore, strongly justify this approach.

Next we enlarge the space of trial overlap functions, and obtain essentially the same result. Working in the single-particle model, we find those potentials that give overlap functions normalized to a spectroscopic factor close to unity and have the asymptotic behavior found experimentally. In the single-particle approach the radial overlap integral is approximated by a single-particle overlap integral

$$I_{Ap l_B j_B}^B(r) \approx I_{Ap l_B j_B}^{B(sp)}(r) = [S_{l_B j_B}^{(sp)}]^{1/2} \psi_{n_B l_B j_B}(r), \tag{6}$$

where ψ is the normalized single-particle radial wave function of the bound state (Ap) calculated in an adopted single-particle potential. At asymptotic distances it behaves like

$$\psi \approx b_{l_B j_B} \frac{W_{\eta_B, l_B + 1/2}(2k_B r)}{r}, \tag{7}$$

where $b_{l_B j_B}$ is the single-particle ANC. The wave function ψ is calculated by adjusting the depth of the potential so that the eigenvalue matches exactly the energy ϵ_B. It follows that the single-particle ANC will depend on all other parameters of the potential. Then $S^{1/2}\psi$ is the required approximation for the overlap integral, and

$$S_{l_B j_B}^{sp} = \left(\frac{C_{l_B j_B}}{b_{l_B j_B}} \right)^2 \tag{8}$$

gives the connection between the single-particle spectroscopic factor, the nuclear ANC, and the single-particle ANC. When the spectroscopic factor of the component containing the ^{7}Be ground state is S_g, one searches for the geometrical parameters of the potential to produce

$$S_g^{1/2} b_{l_B j_B}(R,a) = C_{eff}, \tag{9}$$

where we have explicitly indicated the dependence on the radius R and diffusivity a of the potential. This approach makes sense if the (unknown) spectroscopic factor is close to unity. A complication occurs since the single-particle ANC b_{lj} depends not only on the geometrical parameters, but also on the functional form of the potential. To account for this, we have examined the following functional forms: (a) Woods-Saxon (WS), (b) Gaussian (GS), (c) Morse (MO), and (d) square well (SW). In each case the effective potential consists of a nuclear part, a spin-orbit part, and a Coulomb part. In all cases the spin-orbit term is taken in the usual Thomas form with a strength taken from global parametrizations [24], except for case (d) where we have used $V_{ls} = 0$. In cases (a), (c), and (d) the Coulomb potential is given by the potential of a point charge e interacting with a charge Ze uniformly distributed in a sphere of radius $R_c = R_n$, where R_n is the nuclear radius parameter. In case (b) the Coulomb potential assumes a Gaussian charge distribution of the core. For each functional form of the potential, we search on geometrical parameters in such a way that the quantity

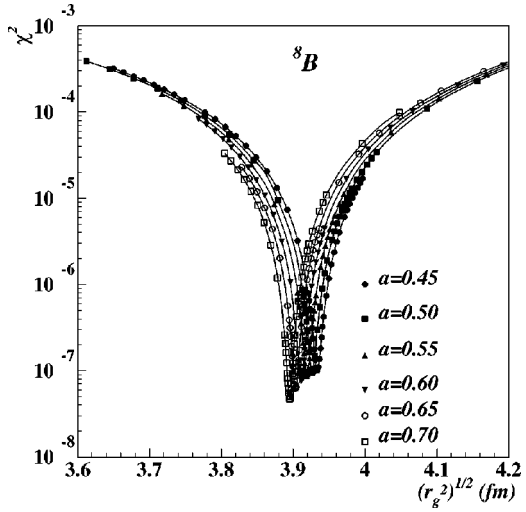

FIG. 1. Dependence of the χ^2 of Eq. (10) on the rms radius of the valence wave function r_g using a Woods-Saxon single-particle potential. Symbols are connected by lines to guide the eye.

$$\chi^2=\sum_{r=R_N}^{40\ \mathrm{fm}}\left(S_g^{1/2}\psi(r_i)-C_{eff}\frac{W(2k_Br_i)}{r_i}\right)^2 \tag{10}$$

becomes minimum. The wave function in Eq. (10) is calculated by the well depth method for quantum numbers $n=0$, $l=1$, $j=3/2$. If $\chi^2\to 0$ for some specific values of geometrical parameters of the potential, then Eq. (10) ensures the convergence in norm. It follows that not only the function and its first derivative is matched to the renormalized Whittaker function, but all derivatives are identical at the matching radius. In practice we have used $R_N=6$ fm, and verified that $R_N=5$ fm does not change the results below.

Results from calculations with Woods-Saxon potentials are displayed in Fig. 1. We use $S_g=0.85$, as suggested by one experiment [25] and in range with some calculations [21,26], but show that the actual value does not matter, as long as it is close to unity. For the diffusivity parameter fixed in the range $a=0.45$–0.70 fm, the radius parameter of the potential is varied in small steps till the absolute minimum in χ^2 is reached. For each pair of parameters, the χ^2 value is plotted as a function of the rms radius of the wave function. The minimum in χ^2 is very deep, dropping by three orders of magnitude compared to adjacent values, pointing to a unique solution of Eq. (9) and a very small dispersion in the rms radius of the wave function. Finally, the average value of the rms radius of the $1p_j$ orbital is calculated by

$$r_1=\sum\ w_i\langle r^2\rangle_i^{1/2},\quad w_i=\frac{\dfrac{1}{\chi_i^2}}{\sum\dfrac{1}{\chi_i^2}}. \tag{11}$$

The sum runs over the 400 wave functions that were calculated.

The same calculations were done for shapes (b)–(d). We obtain essentially the same rms radius for the wave function for all four potential shapes. Therefore, the rms radius of the wave function is nearly model independent.

It is important to estimate the effect of core excitation on the valence proton radius. For this, we write the wave function as

$$|^8\mathrm{B(g.s.)}\rangle=S_g^{1/2}[^7\mathrm{Be}(3/2^-)\otimes p_j]_{2^+}+S_e^{1/2}[^7\mathrm{Be}^*(1/2^-)\otimes p_{3/2}]_{2^+}+\cdots, \tag{12}$$

and then calculate

$$r_h^2=r_g^2+r_e^2+\cdots=\frac{S_g}{S_g+S_e+\cdots}r_1^2+\frac{S_e}{S_g+S_e+\cdots}r_2^2+\cdots, \tag{13}$$

where S_i are the spectroscopic factors and r_i are the rms radii of the corresponding single-particle wave functions. In this convention $S_g+S_e\simeq 1$. To estimate the contribution of core excitation, we calculate the rms radius for a proton wave function in the Woods-Saxon potentials with the same parameters as above, but require its energy to be at $\epsilon_p=-S_p-E^*[^7\mathrm{Be}^*(1/2^-)]=-568$ keV. We get $r_2=3.76$ fm. Microscopic calculations [21,26] find that the ^{7}Be first excited state $J^\pi=1/2^-$ at $E^*=0.429$ keV also contributes. A recent experiment put this contribution at about $S_e/(S_g+S_e)\approx 0.15$ [25]. With this assumption, we estimate that the contribution of the core excitation to the mean square radius [Eq. (4)] is $r_e^2\approx 2.1$ fm^2, using the single-particle model [second term in Eq. (13)]. Including this effect, all methods (grid, WS, GS, MO, SW) give similar results and we find the average rms radius for the last proton in ^{8}B to be $r_h=4.20\pm 0.22$ fm. The individual results are summarized in Table I.

The overlap integrals obtained in the WS calculation are displayed in Fig. 2 and compared with microscopic calculations of Timofeyuk [21]. Those one-nucleon overlap integrals were obtained in a self-consistent many-body calculation using the effective interactions mentioned in the figure. One observes a small dispersion in the interior part of the WS wave functions. They are matched to the renormalized Whittaker function at $R_N=4$ fm, although our matching procedure is performed at 6 fm. Also, one observes that only the M3Y interaction predicts an overlap integral close to ours. All others have too much strength in the asymptotic region, and therefore, do not match the measured ANC.

Assuming a different value for the spectroscopic factor S_g in the procedure outlined above changes the radius r_1 found for the $1p_j$ single-particle orbital, but does not change the result for the contribution of the ^{7}Be ground state to the rms radius of the last proton [r_g in Eq. (13)]. For example, assuming $S_g=1.0$, we obtain $r_g=r_1=4.00\pm 0.20$ fm, very close to what we obtained above. This (r_g^2) is in fact the only contribution to the mean-square radius that we can determine directly from the ANC measured from the peripheral proton transfer reactions, without reference to other experimental results or to model-dependent assumptions.

In order to determine the contribution of the asymptotic part of the wave function to the halo radius, we evaluate

TABLE I. Halo radii r_g and r_h, without and with core excitation contribution, and the matter radius r_m for ^{8}B. The variance is calculated assuming propagation of correlated errors. Lines labeled MB give results from microscopic many-body model calculations with different effective interactions (Minnesota, Hasegawa, M3Y, Volkov). The data labeled ''exp'' are obtained with various models, as described in the references.

Model	r_g [fm]	r_h [fm]	r_m [fm]	Ref.
grid	3.98 ± 0.20	4.23 ± 0.22	2.61 ± 0.04	present
WS	3.91 ± 0.18	4.18 ± 0.20	2.60 ± 0.04	present
GS	3.92 ± 0.18	4.20 ± 0.20	2.60 ± 0.04	present
MO	3.93 ± 0.18	4.21 ± 0.20	2.60 ± 0.04	present
SW	3.97 ± 0.18	4.22 ± 0.20	2.61 ± 0.04	present
aver	3.94 ± 0.20	4.20 ± 0.22	2.60 ± 0.04	present
two-body	3.75		2.51	[27]
RPA+mean field		4.73	2.58	[28]
RGM			2.57	[22]
cluster			2.58–2.60	[26]
cluster			2.56	[29]
cluster			2.73	[20]
MB(Min)		4.40 [a]	2.68 [b]	[21]
MB(Has)		4.43 [a]	2.68 [b]	[21]
MB(M3Y)		4.63 [a]	2.68 [b]	[21]
MB(V2)		4.44 [a]	2.72 [b]	[21]
exp			2.39 ± 0.04	[1]
exp			2.71	[6]
exp	3.97 ± 0.12		2.55 ± 0.08	[5]
exp			2.45 ± 0.10	[30]
exp			2.43 ± 0.03	[31]
exp			2.72	[4]
exp			2.50 ± 0.04	[32]
exp		4.64 ± 0.23	2.83 ± 0.06	[13,2]

[a]Calculated with Eq. (13) using Table II of Ref. [21].
[b]Calculated with Eq. (15).

$$D_\lambda(R_N)=\left[\frac{\int_{R_N}^{\infty} r^{2\lambda}dr\,\psi^2(r)}{\int_0^{\infty} r^{2\lambda}dr\,\psi^2(r)}\right]^{1/\lambda} \tag{14}$$

with $\lambda=1,2$, which measures the contribution of the asymptotic part to the norm and to the rms radius, respectively. For $R_N=4$ fm we find $D_{1(2)}=0.29$ (0.85). Therefore, the asymptotic part of the wave function contributes 85% to the rms radius. Furthermore, if we eliminate the Coulomb field and keep all other parameters of the potential fixed, the rms radius increases to 6.18 fm, which is comparable to that of ^{11}Be [33].

Is ^{8}B a proton-halo nucleus? Although we do not have a clear definition of this phenomenon, it is generally accepted that the fingerprint of a halo nucleus in a ground state is dominated by a weakly bound single- or two-particle component that extends far outside the core. Low angular momentum for low centrifugal barrier and low or no Coulomb barrier are required conditions for this to happen. These

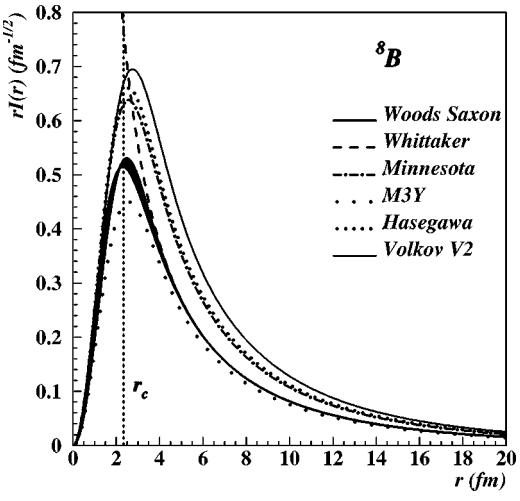

FIG. 2. Overlap integrals $[rI(r)]$ obtained in the minimization procedure of Fig. 1 with a Woods-Saxon potential are compared with the renormalized Whittaker function and with microscopic calculations with various effective interactions [21]. r_c is the radius of the ^{7}Be core.

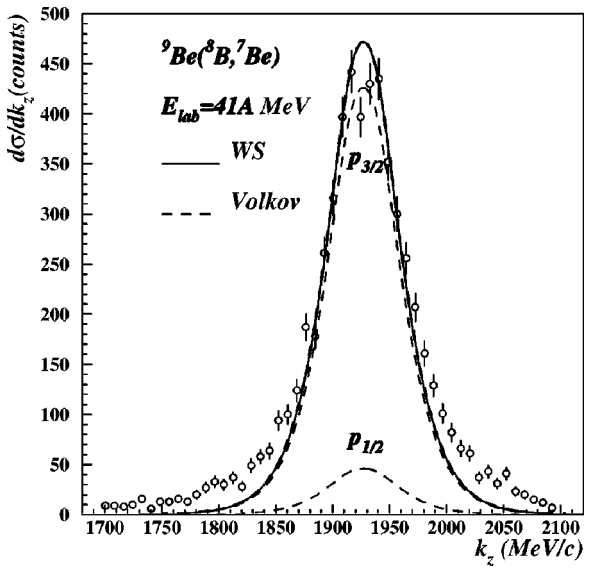

FIG. 3. Parallel momentum distributions for corelike fragments in a breakup reaction of ^{8}B on a ^{9}Be target at 41 MeV/nucleon, calculated in the Hansen model with a Woods-Saxon wave function and with microscopic overlap integral with Volkov force [21], are compared with experimental data [7]. Contributions from $p_{3/2}$ and $p_{1/2}$ states are shown separately for the Volkov force, together with their incoherent sum. Both calculations are normalized to the data. The absolute cross sections are given in Table II.

translate into narrow momentum distributions and large breakup and reaction cross sections as compared to the more bound neighboring nuclei. Typical neutron-halo nuclei are ^{11}Be and ^{11}Li [1]. On the proton-drip-line side, proton haloes are not likely to appear easily due to the strong confinement effect of the Coulomb barrier. We have calculated the intrinsic momentum distribution for the various overlap integrals discussed above. The calculated distributions are indistinguishable up to momenta as large as 200 MeV/c. Beyond this value, the weak dependence of the wave functions on the potential is seen in Fig. 2 and translates into small variations in momentum space that are not observable in a breakup reaction. Therefore, our wave functions give almost the same localization probability in momentum space. The average full widths at half maximum were $\Gamma_t=136$ MeV/c for the total momentum distribution, $\Gamma_z=165$ MeV/c for the parallel momentum distribution, and $\Gamma_r=149$ MeV/c for the radial momentum distribution. The parallel momentum distribution is three times larger than for ^{11}Be. Of course this distribution is strongly filtered by the reaction mechanism in a breakup reaction.

Finally, to study another quantity that is also sensitive to the same one-nucleon overlap integral, we calculate the parallel momentum distribution for corelike fragments in the one-proton breakup reaction of ^{8}B on ^{9}Be and ^{12}C targets using the Hansen model [34]. For these reactions there are experimental data at 40 MeV/nucleon [3] and 41 MeV/nucleon [7]. The calculations are presented in Fig. 3 for one WS wave function and for the many-body overlap integral with the Volkov force. For the latter, the contributions from $p_{3/2}$ and $p_{1/2}$ components are shown separately, together with their incoherent sum. Theoretical distributions that were not corrected for experimental effects are compared to data taken from [7] in the figure. Both theoretical momentum distributions were normalized to the maximum in the experimental data, and they are nearly identical in shape. The shape of the distribution is not able to distinguish between the two functions since both of them reflect the same separation energy and carry the same angular momentum. This entirely determines the shape of the distribution because differences between the two functions in the nuclear interior are obscured by the reaction mechanism [35]. The most important spectroscopic information contained in the wave function is lost by normalizing to the data. The situation is quite different if we look to the total breakup cross section, presented in Table II. As expected, the WS wave function and the M3Y overlap integral, which have similar strengths at asymptotic distances, give similar results. They also reproduce the experimental value, which gives further confirmation for our ^{8}B overlap function obtained from the experimental ANC. In contrast, all other overlap integrals overestimate the experimental value by a factor of 2 or more, and therefore, can be ruled out.

We conclude that the above are strong arguments for ^{8}B being a halo nucleus. Taking $R_N=2.5$ fm in Eq. (14), slightly larger than the radius of the ^{7}Be core [1], we find $D_{1(2)}=0.64$ (0.90). Therefore, the probability to find the last proton outside the ^{7}Be core is around 65%. Contributions from clusterlike configurations, not considered here, to the ground state of ^{8}B cannot change significantly the above conclusions.

These findings also allow us to estimate the matter radius of the ^{8}B nucleus according to [36]:

$$r_m^2=\frac{1}{A+1}\left(Ar_c^2+r_p^2+\frac{A}{A+1}r_h^2\right), \tag{15}$$

where $r_c=2.33\pm0.02$ fm is the experimentally measured rms radius of the core nucleus ^{7}Be [1], $r_p=0.81$ fm is the

TABLE II. Calculated total breakup cross section (σ_{-1p}) for the reaction ^{8}B+^{12}C$\rightarrow^7$Be+$\cdots$ at 40 MeV/nucleon and full width at half maximum for the parallel momentum distribution Γ_z in the reaction ^{8}B+^{9}Be$\rightarrow^7$Be+$\cdots$ at 41 MeV/nucleon.

	WS	M3Y	Minnesota	Hasegawa	Volkov	Exp.
σ_{-1p} (mb)	97.5	96.6	176.0	213.8	266.9	80±15 [3]
Γ_z (MeV/c)	73.2	73.1	73.2	72.9	73.3	81±4 [7]

proton radius, and r_h is the halo radius from Table I. This formula assumes that ^{7}Be behaves identically inside ^{8}B as the free ^{7}Be and accounts of the recoil effect of the ^{8}B center of mass with respect to the ^{7}Be core. The extracted rms radius of ^{8}B is $r_m = 2.60 \pm 0.04$ fm. Further contributions from clusterlike components in the ^{8}B wave function will modify this value, but we cannot estimate their contribution. However, we note that this simple estimate compares well with experimental measurements (see Table I) and agrees with the values given by far more sophisticated RGM and many-body calculations [21,22,26,28,29]. Note that, in fact, all radii labeled ''exp'' in Table I are model dependent, and the assumptions vary from case to case. The advantage of the present approach for obtaining the rms radius of ^{8}B over more complete many-body treatments stems from the fact that it matches the experiment, through the ANC, the part that contributes most: the asymptotic part of the one-nucleon overlap integral. This is possible only for halo nuclei.

In summary, we have examined the possibility to extract valuable information regarding the wave function of ^{8}B from the experimentally measured asymptotic normalization coefficient. Under favorable circumstances (very low separation energy and a spectroscopic factor close to 1), we have shown that the rms radius of the last proton can be determined. We have shown that this result is independent of the functional form of the potential and its geometrical parameters. We obtain an rms radius of 4.20 ± 0.22 fm for the last proton in ^{8}B, which shows that on average it is localized at a distance two times larger than the size of the core. The effect is entirely due to the very low binding energy of the last proton. Core excitation effects on the halo radius are included, but they represent only a small correction. The asymptotic part of the wave function contributes about 85% to the orbit radius. When combined with the experimentally measured radius of the core nucleus ^{7}Be, the radius of ^{8}B is close to values extracted from reaction and interaction cross sections and agrees with that obtained in sophisticated RGM and many-body calculations. The consistency of our overlap integral with the measured parallel momentum distribution and total breakup cross section was also verified. The halo nature of ^{8}B seems firmly established.

We thank N. K. Timofeyuk for correspondence. One of us (F.C.) thanks the Cyclotron Institute, Texas A & M University for the hospitality and support extended for the visit during which a part of this work was completed. This work was supported in part by the U.S. Department of Energy under Grant No. DE-FG03-93ER40773 and by the Robert A. Welch Foundation.

[1] I. Tanihata, T. Kobayashi, O. Yamakawa, S. Shimoura, K. Ekuni, K. Sugimoto, N. Takahashi, and T. Shimoda, Phys. Lett. B **206**, 592 (1988).
[2] B. Blank *et al.*, Nucl. Phys. **A624**, 242 (1997).
[3] I. Pecina *et al.*, Phys. Rev. C **52**, 191 (1995).
[4] R. E. Warner *et al.*, Phys. Rev. C **52**, R1166 (1995).
[5] F. Negoita *et al.*, Phys. Rev. C **54**, 1787 (1996).
[6] T. Minamisono *et al.*, Phys. Rev. Lett. **69**, 2058 (1992).
[7] J. H. Kelley *et al.*, Phys. Rev. Lett. **77**, 5020 (1996).
[8] T. Motobayashi *et al.*, Phys. Rev. Lett. **73**, 2680 (1994).
[9] B. Davids *et al.*, Phys. Rev. Lett. **81**, 2209 (1998).
[10] N. Iwasa *et al.*, Phys. Rev. Lett. **83**, 2910 (1999).
[11] K. Hencken, G. Bertsch, and H. Esbensen, Phys. Rev. C **54**, 3043 (1996).
[12] R. Shyam and I. J. Thompson, Phys. Rev. C **59**, 2645 (1999).
[13] H. Esbensen and K. Hencken, Phys. Rev. C **61**, 054606 (2000).
[14] M. H. Smedberg *et al.*, Phys. Lett. B **452**, 1 (1999).
[15] A. Azhari, V. Burjan, F. Carstoiu, H. Dejbakhsh, C. A. Gagliardi, V. Kroha, A. M. Mukhamedzhanov, L. Trache, and R. E. Tribble, Phys. Rev. Lett. **82**, 3960 (1999).
[16] A. Azhari, V. Burjan, F. Carstoiu, C. A. Gagliardi, V. Kroha, A. M. Mukhamedzhanov, X. Tang, L. Trache, and R. E. Tribble, Phys. Rev. C **60**, 055803 (1999).
[17] A. Azhari, V. Burjan, F. Carstoiu, C. A. Gagliardi, V. Kroha, A. M. Mukhamedzhanov, X. Tang, L. Trache, and R. E. Tribble, Phys. Rev. C (to be published).
[18] G. R. Satchler, *Direct Nuclear Reactions* (Clarendon, New York, 1983).
[19] H. M. Xu, C. A. Gagliardi, R. E. Tribble, A. M. Mukhamedzhanov, and N. K. Timofeyuk, Phys. Rev. Lett. **73**, 2027 (1994).
[20] D. Baye, P. Descouvemont, and N. K. Timofeyuk, Nucl. Phys. **A577**, 624 (1994); **A588**, 147c (1995).
[21] N. K. Timofeyuk, Nucl. Phys. **A632**, 19 (1998).
[22] A. Csótó, Phys. Lett. B **315**, 24 (1993).
[23] A. M. Mukhamedzhanov, C. A. Gagliardi, and R. E. Tribble, Phys. Rev. C **63**, 024612 (2001).
[24] F. D. Becchetti and G. W. Greenlees, Phys. Rev. **182**, 1190 (1969).
[25] K. Markenroth *et al.*, International Symposium on Perspectives Physics Radioactive Isotope Beams, Hayama, Japan, 2000, contribution C-17.
[26] L. V. Grigorenko, B. V. Danilin, V. D. Efros, N. B. Shul'gina, and M. V. Zhukov, Phys. Rev. C **57**, R2099 (1998); **60**, 044312 (1999).
[27] K. Riisager and A. S. Jensen, Phys. Lett. B **301**, 6 (1993).
[28] H. Lenske, J. Phys. G **24**, 1429 (1998); T. Baker *et al.*, Phys. Rep. **289**, 235 (1997).
[29] K. Varga, Y. Suzuki, and I. Tanihata, Phys. Rev. C **52**, 3013 (1995).
[30] M. Fukuda *et al.*, Nucl. Phys. **A656**, 209 (1999).
[31] M. M. Obuti *et al.*, Nucl. Phys. **A609**, 74 (1996).
[32] J. S. Al-Khalili and J. A. Tostevin, Phys. Rev. Lett. **76**, 3903 (1996).
[33] T. Nakamura *et al.*, Phys. Lett. B **331**, 296 (1994).
[34] P. G. Hansen, Phys. Rev. Lett. **77**, 1016 (1996).
[35] W. Schwab *et al.*, Z. Phys. A **350**, 283 (1995).
[36] B. Buck and A. A. Pilt, Nucl. Phys. **A280**, 133 (1977).